J Biomol NMR (2013) 55:279–289
DOI 10.1007/s10858-013-9711-4

ARTICLE

Probing slowly exchanging protein systems via $^{13}C^{\alpha}$-CEST: monitoring folding of the Im7 protein

Alexandar L. Hansen · Guillaume Bouvignies · Lewis E. Kay

Received: 5 December 2012 / Accepted: 20 January 2013 / Published online: 6 February 2013

Abstract A $^{13}C^{\alpha}$ chemical exchange saturation transfer based experiment is presented for the study of protein systems undergoing slow interconversion between an 'observable' ground state and one or more 'invisible' excited states. Here a labeling strategy whereby [2-^{13}C]-glucose is the sole carbon source is exploited, producing proteins with ^{13}C at the C^{α} position, while the majority of residues remain unlabeled at CO or C^{β}. The new experiment is demonstrated with an application to the folding reaction of the Im7 protein that involves an on-pathway excited state. The obtained excited state $^{13}C^{\alpha}$ chemical shifts are cross validated by comparison to values extracted from analysis of CPMG relaxation dispersion profiles, establishing the utility of the methodology.

Keywords Protein dynamics · Slow chemical exchange · Chemical exchange saturation transfer (CEST) · Protein folding · Im7

Introduction

Much of structural biology has focused on studies of highly populated, long-lived conformers that can be readily characterized using a wide array of powerful biochemical and biophysical methods. It is increasingly clear, however, that additional conformations, beyond that of the ground state, can be critical for function (Ishima et al. 1999; Karplus and Kuriyan 2005; Boehr and Wright 2008; Fraser et al. 2009). Often these conformers are sparsely and transiently populated (so called excited conformational states) so that they evade detection by conventional biophysical techniques. In principle, solution NMR spectroscopy is a powerful method for studies of such elusive conformations and the basic 'experimental building blocks' for doing so were developed already 50 years ago! More recently, experiments such as Carr-Purcell-Meiboom-Gill (CPMG) relaxation dispersion (Carr and Purcell 1954; Meiboom and Gill 1958; Allerhand and Gutowsky 1964), $R_{1\rho}$ relaxation (Deverell et al. 1970) and Chemical Exchange Saturation Transfer (CEST) (Forsén and Hoffman 1963) have been significantly modified for studies of biomolecules such as proteins and nucleic acids (Palmer et al. 2005; Palmer and Massi 2006; Hansen et al. 2008a, 2009; Vallurupalli et al. 2008, 2012; Fawzi et al. 2011).

Central to the success of such methods is the fact that they report not only on the kinetics and thermodynamics of exchange processes but also on the chemical shifts of 'invisible' excited states that interconvert with 'visible' ground state conformers. In parallel with the development of the experimental toolkit for extracting chemical shifts has been the emergence of computational methods for converting these shifts into detailed structural information. Once chemical shifts can be obtained, modern prediction tools such as Sparta+ (Shen and Bax 2010), Shiftx+ (Han

Electronic supplementary material The online version of this article (doi:10.1007/s10858-013-9711-4) contains supplementary material, which is available to authorized users.

A. L. Hansen · G. Bouvignies · L. E. Kay (✉)
Departments of Molecular Genetics, Biochemistry and Chemistry, The University of Toronto, Toronto, ON M5S 1A8, Canada
e-mail: kay@pound.med.utoronto.ca

L. E. Kay
Hospital for Sick Children, Program in Molecular Structure and Function, 555 University Avenue, Toronto, ON M5G 1X8, Canada

et al. 2011) or Camshift (Kohlhoff et al. 2009), for example, can be used in conjunction with molecular dynamics simulations (Robustelli et al. 2010; Camilloni et al. 2012), database protocols such CS-Rosetta (Lange et al. 2012), CHESIRE (Cavalli et al. 2007) or CS23D (Wishart et al. 2008), or with structure prediction programs (Parisien and Major 2008) to determine the structures of these invisible, excited states (Vallurupalli et al. 2008; Korzhnev et al. 2010; Bouvignies et al. 2011; Nikolova et al. 2011; Dethoff et al. 2012; Neudecker et al. 2012).

Over the past 15 years our laboratory has focused on developing a suite of CPMG relaxation dispersion experiments for studies of exchanging protein systems using backbone (Orekhov et al. 2004; Lundström et al. 2008, 2009; Hansen et al. 2008b, c) and side-chain (Korzhnev et al. 2005; Lundström et al. 2007a, b; Hansen and Kay 2011; Hansen et al. 2012) ^{1}H, ^{13}C and ^{15}N probes with the goal of providing the framework for detailed structural studies of excited protein conformers. The CPMG technique is sensitive to exchange over a relatively narrow window, from approximately 200–2,000 s^{-1}. We have shown that it is possible to extend the upper boundary of the exchange time-scale to 5,000–6,000 s^{-1}, through a combination of experiments that monitor both transverse relaxation rates (CPMG) and the static field dependence of the ground state peak positions (Vallurupalli et al. 2011). Exchanging systems that interconvert with rates on the order of 100 s^{-1} or less and where excited state conformations remain invisible have proven difficult to study in the past. However, the development of CEST methods provides an avenue for detailed characterization of excited states in this case as well. In an important application of the CEST methodology to macromolecules, Fawzi et al. (2011) have developed an ^{15}N-based experiment and used it to measure (1) the interconversion of the Alzheimer's Aβ peptide between the free form and high molecular weight protofibrils and (2) the ^{15}N linewidths of the invisible fibril state resonances. Our laboratory has described a related ^{15}N-CEST scheme (Vallurupalli et al. 2012) for measurement of chemical shifts of excited states, ensuring that the ^{15}N lines could be properly decoupled from the one-bond $^{1}H^{N}$–^{15}N scalar couplings during CEST evolution without the introduction of sidebands. Very recently, schemes for $^{13}CH_3$-CEST (Bouvignies and Kay 2012a) and $^{1}H^{N}$-CEST (Bouvignies and Kay 2012b), as applied to proteins, have been proposed as well.

It has long been recognized that the $^{13}C^{\alpha}$ chemical shift is a sensitive and perhaps the most significant reporter of protein backbone secondary structure (Spera and Bax 1991; Wishart and Sykes 1994). On the basis of a range of studies, extending from empirical observations (Spera and Bax 1991) to DFT calculations (Vila and Scheraga 2009), the $^{13}C^{\alpha}$ shift has been shown to be largely determined by residue type and backbone conformation with much less dependence on side-chain geometry, primary sequence or oligomerization state (Iwadate et al. 1999; Vila et al. 2007). In studies of excited protein states, knowledge of the $^{13}C^{\alpha}$ shifts is, not surprisingly, often critical for accurate structure determination. With this in mind, we extend the CEST toolkit for studies of slowly exchanging states by presenting a $^{13}C^{\alpha}$-based experiment. The methodology is applied to study the folding of a small 87 residue protein, the colicin E7 immunity protein (Im7) (Capaldi et al. 2002; Papadakos et al. 2012). We discuss the reliability of extracted parameters such as the rates of exchange and the populations of exchanging states and evaluate the accuracy of the measured chemical shifts by comparison with corresponding values that are obtained via CPMG relaxation dispersion.

Materials and methods

Protein sample preparation

Isotopically enriched samples of wild-type Im7 were expressed in protonated M9 minimal media, using 3 g/L of [2-^{13}C]-glucose (Lundström et al. 2007a; Hansen et al. 2008c) and 1 g/L of $^{15}NH_4Cl$ as the sole carbon and nitrogen sources, respectively, and purified as described previously (Hansen and Kay 2011). A lyophilized sample of Im7 was dissolved in NMR buffer containing 50 mM potassium phosphate, pH 6.6, 0.03 % sodium azide, and 100 % D_2O to a concentration of 1.4 mM in protein and used for this work.

NMR spectroscopy

2D $^{13}C^{\alpha}$-CEST experiments were recorded (5 °C) on spectrometers operating at 14.1 T and 18.8 T, equipped with cryogenically cooled (14.1 T) and room temperature (18.8 T) probes. A number of experimental datasets were obtained, corresponding to weak $^{13}C^{\alpha}$ B_1 fields of ~15, 25, and 100 Hz, as summarized in Table 1. The B_1 field strengths were calibrated by monitoring a single, on-resonance signal and varying T_{Ex} (Fig. 1) according to the procedure of Guenneugues et al. (1999). Calibrated field strengths were found to be 15.5 (15.8), 26.7 (27.6), and 104.5 (107.3) Hz at 14.1 (18.8) T. Spectra were recorded with acquisition parameters listed in Table 1, 15–45 min per 2D plane, $(t_{1,\max}, t_{2,\max}) \approx$ (16–18 ms, 64 ms) and total measurement times of 1–2 days per CEST data set. A single spectrum was recorded with $T_{Ex} = 0$ for each CEST data set to estimate $^{13}C^{\alpha}$ R_1 values of the ground state. $^{13}C^{\alpha}$ CPMG relaxation dispersion data sets were acquired (25 °C) as described previously (Hansen et al. 2008c), using the same sample as for the CEST measurements.

Table 1 Experimental parameters for recording $^{13}C^{\alpha}$ CEST data sets, Im7, 5 °C using the scheme of Fig. 1

B_o (T)	B_1 (Hz)[a]	T_{Ex} (ms)	Scans[b]	Complex t_1 points	# planes[c]	Step size (Hz)[c]	Total time (hours)[d]
14.1	15	700	4	48	101	35	30.2
	25	700	4	48	101	35	30.2
	100	350	8	54	42	100	28.3
18.8	15	600	4	52	181	22	56.5
	25	600	4	46	111	35	30.7
	100	350	8	64	55	100	42.3

[a] Strength (Hz) of weak $^{13}C^{\alpha}$ B_1 field applied during T_{Ex} (see Fig. 1)

[b] Number of transients recorded for each FID

[c] Number of 2D ^{13}C-^{1}H planes recorded in each CEST data set; for each plane a weak B_1 field is applied at a particular $^{13}C^{\alpha}$ frequency. In each successive plane the position of the applied B_1 field is incremented by the amount indicated (Step size, Hz)

[d] Net measurement time for a CEST data set

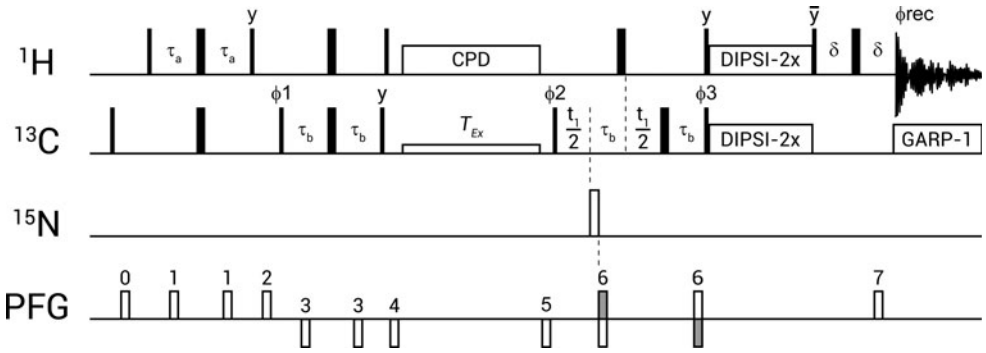

Fig. 1 Pulse sequence for the measurement of $^{13}C^{\alpha}$-CEST profiles using protein samples with selective labeling at the $^{13}C^{\alpha}$ position as described in the text. Narrow and wide solid *rectangles* denote high power 90° and 180° pulses, respectively. The ^{1}H carrier is centered on the water signal ($^{1}H^{\alpha}$ region) while the ^{13}C transmitter is positioned at 61 ppm ($^{13}C^{\alpha}$), with the exception of the interval corresponding to T_{Ex} where the placement of the ^{13}C carrier varies from one 2D spectrum to the next. The ^{15}N pulse is applied as $90_x240_y90_x$ (Freeman et al. 1980), centered at 119 ppm. Delay times are $\tau_a = 1.6$–1.8 ms $\approx 1/(4J_{CH})$, $\tau_b = 1.78$ ms $= 1/(4J_{CH})$, $\delta = 450$ µs, and DIPSI-2 transfer element ($\sim$7.5 kHz ^{1}H and ^{13}C fields) = 7.7 ms $\approx 1/J_{CH}$ (Shaka et al. 1988). The weak CW B_1 RF field utilized during the CEST relaxation element (15–100 Hz) is applied for a time T_{Ex} (350–700 ms in the present study), with ^{1}H decoupling achieved with a 3.6 kHz $90_x240_y90_x$ sequence (Levitt 1982) as described by Vallurupalli et al. (2012). A 2.9 kHz GARP (Shaka et al. 1985) decoupling field is used during acquisition. All pulses are x phase unless otherwise noted. A 4-step phase cycle is utilized with $\phi1 = x, -x$, $\phi2 = 2(y), 2(-y)$, $\phi3 = y$, $\phi rec = -x, 2(x), -x$. Quadrature detection in the indirect dimension is achieved using an enhanced sensitivity gradient scheme (Kay et al. 1992; Schleucher et al. 1993) whereby both cosine and sine modulated $^{13}C^{\alpha}$ magnetization components are transferred to observable magnetization via a planar-TOCSY scheme (Sattler et al. 1999) by recording a pair of spectra for each t_1 value with ($\phi3$, g6) and ($\phi3 + 180°$, −g6). Axial peaks are shifted to the edge of the spectrum by incrementing $\phi2$ and ϕrec by 180° with each successive t_1 value (Marion et al. 1989). Gradient strengths in G/cm (lengths in ms) are: 0 = 15 (1), 1 = 20 (0.5), 2 = 30 (0.8), 3 = −8 (0.6), 4 = − 32 (1), 5 = − 20 (0.7), 6 = 30 (0.2), and 7 = 29.6 (0.1)

Data analysis

Spectra were processed and analyzed using the NMRPipe suite of programs (Delaglio et al. 1995) and visualized using Sparky (Kneller and Kuntz 1993). Very weak decoupling sideband artifacts were observed, as described in the text and elsewhere (Vallurupalli et al. 2012). Because their position can be calculated accurately, we have removed the one or two points that define these sideband frequencies from each profile prior to analysis. Note that this did not compromise the analysis of the data because the positions of the sidebands did not interfere with major or minor state dips. This was achieved by adjusting the ^{1}H decoupling field strength so that sidebands appeared at frequencies larger than $\pm|\Delta\varpi|$ from the major state dip, as described below. Profiles were subsequently fit to a two-site exchange model between ground (G) and excited (E) states, $G \underset{k_{EG}}{\overset{k_{GE}}{\rightleftharpoons}} E$, using an in-house program for numerical fitting of the Bloch-McConnell equations (McConnell 1958), as discussed previously (Vallurupalli et al. 2012), that is available upon request. Fitting parameters include the per residue values, $\{I_0, \varpi_G, \Delta\varpi = \varpi_E - \varpi_G, R_1, R_{2,G}, \Delta R_2 = R_{2,E} - R_{2,G}\}$ and global parameters

Table 2 Global exchange parameters obtained from fits of Im7 CEST profiles using subsets of the acquired data as indicated, 5 °C

Dataset		k_{ex} (s^{-1})	p_E (%)
B_o (T)	B_1 (Hz)		
14.1	15 + 25	106.7 ± 9.3	1.041 ± 0.032
	15 + 25 + 100	127.5 ± 5.5	0.980 ± 0.017
18.8	15 + 25	78.2 ± 9.1	1.120 ± 0.051
	15 + 25 + 100	140.5 ± 5.7	0.958 ± 0.020
14.1 + 18.8	15 + 25	100.0 ± 6.9	1.057 ± 0.026
	15 + 25 + 100	135.0 ± 3.9	0.965 ± 0.012

$\{k_{ex} = k_{GE} + k_{EG}, p_E\}$, where I_0 is a scaling factor for each profile, R_1 is the $^{13}C^{\alpha}$ longitudinal relaxation rate that is assumed the same for corresponding nuclei in ground and excited states, $R_{2,G}$ is the transverse relaxation rate of a spin in the ground state and the fractional population of the excited state is given by p_E. Previously described simulations by Fawzi et al. (2011) and by our group (Vallurupalli et al. 2012) have established that the extracted exchange parameters as well as chemical shifts of the excited state are little effected by differences in R_1 values between ground and excited states. Values of ΔR_1 on the order of 2 s^{-1} are calculated for changes in correlation time from ~10 ns (Im7 at 5 °C, 18.8T) to 2 ns that might reflect an order–disorder transition; even for such relatively large changes in tumbling times the resultant CEST profiles remain essentially unchanged, and hence the extracted parameters and shift differences are unaffected. Of the 65 CEST profiles obtained, 12 derive from residues with large $^{13}C^{\alpha}$ $\Delta\varpi$ values, $|\Delta\varpi| > 2$ ppm (I22, E26, T30, F41, V42, K43, T45, H47, T51, D52, I54, and Y55); these were chosen to define the global parameters, Table 2. Once determined, the global parameters were then fixed and CEST profiles from the remaining 53 residues were fit to extract accurate $\Delta\varpi$ values. Errors in the extracted parameters were estimated based on their covariance (Press et al. 2007). $^{13}C^{\alpha}$ CPMG dispersion profiles were analyzed as described previously (Hansen and Kay 2011).

Even from a visual inspection of the CEST profiles, focusing on those for which $|\Delta\varpi| > 2$ ppm, it was clear that for some residues $\Delta R_2 > 0$. Of the 12 residues considered initially, a $\Delta R_2 > 0$ value was required for five (T30, F41, V42, K43, and Y55, based on individual fits with and without ΔR_2), providing strong evidence of a third conformer that is in fast exchange with the excited state (see "Results and discussion"). A grid search over global parameters k_{ex} and p_E was performed using the 7 residues with large values of $\Delta\varpi$ and $\Delta R_2 \sim 0$ to define the intrinsic uncertainties in the global parameters.

Monte Carlo simulations (Press et al. 2007) were used to investigate the effect of a third state on the obtained global parameters. Synthetic 2-state data were generated with $\{k_{ex}, p_E\} = \{100\ s^{-1},\ 1.0\ \%\}$ and $\Delta\varpi = \{-4.0, -3.0, -2.0, -1.0, 1.0, 2.0, 3.0, 4.0\}$ ppm and fitted with a model of 2-site exchange as a control. Subsequently a 3-state model, $G \underset{k_{E1G}}{\overset{k_{GE1}}{\rightleftharpoons}} E1 \underset{k_{E2E1}}{\overset{k_{E1E2}}{\rightleftharpoons}} E2$ was used in calculations with $\{k_{ex,GE1}, p_{E1}, k_{ex,E1E2}, p_{E2}\} = \{100\ s^{-1},\ 1.0\ \%,\ 2{,}000\ s^{-1},\ 0.45\ \%\}$, $\Delta\varpi_{G,E1} = \Delta\varpi = \varpi_{E1} - \varpi_G$, $\Delta\varpi_{G,E2} = \varpi_{E2} - \varpi_G = \{2.5, 2.5, -0.5, 2.0, -3.0, -1.0, 1.5, -1.0\}$ ppm. Gaussian error (1.3 % of the reference experiment peak intensities) was added to each point of the CEST profiles; 1000 such data sets were generated and each fit using the same protocol as for the real data. For comparison with the 'in-silico' generated data, Monte Carlo simulations were also carried out using the best-fit solutions to the experimental data (fits of profiles corresponding to the 12 Im7 residues with $|\Delta\varpi| >$ 2 ppm) and the experimentally determined intensity errors. The $\{k_{ex}, p_E\}$ pairs obtained from all fits are plotted to generate distributions of exchange parameters, as described in the text.

Results and discussion

Measurement of invisible state $^{13}C^{\alpha}$ shifts: a strategy

There are a number of different labeling strategies suitable for proteins that are to be studied via $^{13}C^{\alpha}$-CEST. One approach is to prepare uniformly ^{13}C labeled proteins using standard ^{13}C-glucose as the sole carbon source. This has the advantage in that all C^{α} positions are ^{13}C labeled at a level of close to 100 % but results in a number of disadvantages. First, for many amino acid types it is not possible to remove the $^{13}C^{\alpha}$–$^{13}C^{\beta}$ couplings in a straightforward manner, necessitating the use of constant-time based methods (Santoro and King 1992; Vuister and Bax 1992) for recording the $^{13}C^{\alpha}$ chemical shift in the indirect dimension of 2D ^{13}C-^{1}H correlation maps. This leads naturally to a reduction in sensitivity, especially for exchanging systems. In addition, the $^{13}C^{\alpha}$–^{13}CO and $^{13}C^{\alpha}$–$^{13}C^{\beta}$ couplings lead to peak broadening of the $^{13}C^{\alpha}$ correlations in the CEST dimension of the experiment (see below) or possibly to the appearance of peak splittings that further attenuate the signal.

A second labeling strategy is possible that exploits a different carbon source, [2-^{13}C]-glucose. As has been described previously, proteins produced in this manner are labeled with ^{13}C at the C^{α} position, but for the most part not at CO or C^{β} (Lundström et al. 2007a). We have shown that the extent of labeling at C^{α} ranges from 20 to 40 % for all amino acids, with the exception of Leu that is not labeled using this procedure, while some labeling at C^{β} is also observed for Ile and Val. The presence of $^{13}C^{\alpha}$–$^{13}C^{\beta}$

spin pairs is particularly detrimental for the CPMG class of experiment because magnetization originating on $^{13}C^{\alpha}$ can be transferred via a Hartmann-Hahn effect to coupled $^{13}C^{\beta}$ spins in a manner which depends on the rate of application of the CPMG refocusing pulses (Ishima et al. 2004; Lundström et al. 2008). By contrast, the CEST experiment is much more forgiving, as only a very weak $^{13}C^{\alpha}$ B_1 field (typically 20–50 Hz) is applied during a delay that transfers magnetization between exchanging states (see below). Therefore, while additional couplings will lead to peak broadening they will not prevent accurate measurement of excited state chemical shifts. We have chosen to use this labeling approach here.

Figure 1 illustrates the pulse scheme that has been developed for recording $^{13}C^{\alpha}$ CEST profiles of proteins expressed with [2-^{13}C]-glucose. The magnetization transfer pathway can be summarized as follows,

$$^{1}H^{\alpha} \xrightarrow{J_{C^{\alpha}H^{\alpha}}} {}^{13}C^{\alpha} \rightarrow CEST(T_{Ex}) \rightarrow {}^{13}C^{\alpha}(t_1) \xrightarrow{J_{C^{\alpha}H^{\alpha}}} {}^{1}H^{\alpha}(t_2), \quad (1)$$

with the scalar couplings responsible for magnetization transfers indicated above the arrows and t_1, t_2 denote evolution periods where chemical shifts are recorded. During the $CEST(T_{Ex})$ period, $^{13}C^{\alpha}$ longitudinal magnetization is perturbed through the application of a weak B_1 field for a time T_{Ex}; because the magnetization of interest is along Z and $T_1 >> T_2$ in biomolecular systems, values of T_{Ex} on the order of several hundreds of milliseconds can be used, an order of magnitude longer than the CPMG interval. In the event that the weak B_1 field is centered on an excited state resonance, exchange leads to attenuation of the longitudinal magnetization from the ground state spin and hence a decrease in its cross peak intensity in the 2D ^{13}C-^{1}H correlation map. A large number of such maps are recorded with the position of the weak B_1 field systematically varied over the $^{13}C^{\alpha}$ spectral range. Normalized intensities of cross peaks are plotted as a function of the position of the carrier, as illustrated below (I/I_o, where I and I_o are intensities of cross peaks in spectra measured with the chosen T_{Ex} value and $T_{Ex} = 0$, respectively). Because relatively long T_{Ex} values can be selected, slowly exchanging systems can be studied using this approach (Fawzi et al. 2011; Bouvignies and Kay 2012a; Vallurupalli et al. 2012; Bouvignies and Kay 2012b).

In order to maximize sensitivity, it is important to efficiently decouple the $^{1}H^{\alpha}$ spins from $^{13}C^{\alpha}$. In a typical ^{13}C-observe experiment ^{1}H decoupling is most readily achieved using a composite-pulse scheme such as WALTZ (Shaka et al. 1983) or GARP (Shaka et al. 1985) and the very small modulation sidebands that sometimes result are typically not a problem. The situation is somewhat different in the CEST experiment because small peaks that are connected with the major resonance derived from the ground state are amplified very considerably. For example, despite the fact that the fractional population of the excited state, p_E, may be only 1 % that of the ground state, resonances from the excited state are clearly observed because of the long CEST relaxation period, T_{Ex}, during which a weak ^{13}C B_1 field is applied. When the position of such a field coincides with a decoupling sideband, it will similarly lead to a significant perturbation of the ground state resonance. As a result, we have employed a $90_x240_y90_x$ composite decoupling scheme (Levitt 1982), described previously (Vallurupalli et al. 2012), where the first set of (very weak) sidebands are observed at $\pm 0.43\ B_1$ (in Hz) from the major state resonance. By using a 3.5 kHz ^{1}H field, ^{13}C sidebands are predicted at ± 7.5 ppm from the ground state correlation for measurements at 18.8T (and further for smaller B_o), well removed from peaks derived from the excited state even in the case of large conformational changes.

An application of the $^{13}C^{\alpha}$-CEST experiment to folding of the Im7 protein

Many proteins, including those that are relatively small and comprise only a single domain, have been shown to fold via intermediates that are transiently formed and only sparsely populated (Bai et al. 1995; Capaldi et al. 2002; Daggett and Fersht 2003; Korzhnev et al. 2004; Brockwell and Radford 2007; Korzhnev et al. 2010). Detailed structural studies of such intermediates not only inform on basic principles of protein folding but, in some cases, may also provide important clues as to how proteins misfold (Chiti and Dobson 2006; Neudecker et al. 2012). One protein that our laboratory has been studying is the four helix bundle Im7 that folds via an on-pathway intermediate (Capaldi et al. 2001) and we have applied the $^{13}C^{\alpha}$-CEST methodology presented above to this system. Figure 2a shows the ^{13}C-^{1}H correlation map of Im7, 18.8 T, 5 °C recorded with the scheme of Fig. 1, $T_{Ex} = 0$. Notably, a significant variation in cross peak intensities is observed that reflects the different efficiencies of ^{13}C labeling at C^{α} positions of different residues (Lundström et al. 2007a). Representative CEST profiles are shown in Fig. 2b obtained with T_{EX} values ranging between 350 and 700 ms and $^{13}C^{\alpha}$ B_1 field strengths of 15, 25 and 100 Hz, as indicated in Table 1. As the B_1 field increases, the profile dips become broader as discussed previously (Vallurupalli et al. 2012). Also apparent, is the fact that there can be very considerable differences in linewidths between ground and excited state correlations, as observed for T30 (excited state resonance indicated by *). Indeed, differences in relaxation rates, $\Delta R_2 = R_{2,E} - R_{2,G}$, obtained from fits assuming a two-site exchange process, range from 0 to 800 s^{-1}, for the 12 residues with clear minor state dips ($|\Delta\varpi| = |\varpi_E - \varpi_G| > 2$ ppm), with median values of 195 and 317 s^{-1} at 14.1 and 18.8 T, respectively. One possibility is that the

excited state is an aggregate, however the wide distribution of ΔR_2 values argues against this possibility. Additionally, CPMG dispersion profiles recorded as a function of protein concentration are indistinguishable, suggesting that the exchange process does not involve changes in oligomerization state. $^{13}C^{\alpha}$ ΔR_2 values obtained from fits of CEST profiles recorded at 14.1 and 18.8 T are highly correlated with a slope of ca. 16/9 that is predicted in the case of fast chemical exchange (see Supporting information). This suggests that there is an additional exchange process involving a second excited conformer, $E2$, ($G \underset{k_{E1G}}{\overset{k_{GE1}}{\rightleftharpoons}} E1 \underset{k_{E2E1}}{\overset{k_{E1E2}}{\rightleftharpoons}} E2$) that is much faster than the $G \longleftrightarrow E1$ interconversion, giving rise to a single and often significantly broadened dip for each excited state $^{13}C^{\alpha}$. Note that the relative order of $E1$ and $E2$ in the above scheme is not known based on our limited data.

In an effort to understand how the additional exchange process influences extracted rates and populations from fits of CEST data to a 2-site exchange model that includes a ΔR_2 term, we have carried out a number of Monte Carlo simulations using parameters described in "Materials and methods". As expected, if the process is truly 2-site exchange, $G \underset{k_{EG}}{\overset{k_{GE}}{\rightleftharpoons}} E$, then fits of CEST data produce accurate values of p_E and $k_{ex} = k_{GE} + k_{EG}$, Fig. 3a. Moreover, the extracted values are independent of what B_1 fields are used to record the data, as expected (compare blue and red in Fig. 3, corresponding to $B_1 = \{15, 25\}$ Hz and $B_1 = \{15, 25, 100\}$ Hz, respectively).

In the limiting case where the exchange between $E1$ and $E2$ becomes very fast the exchange process can again be well modeled by a 2-site interconversion with an effective population of the excited state given by $p_{E1} + p_{E2}$ and an effective exchange rate that is less than $k_{GE1} + k_{E1G}$. In the general case, if a 2-site exchange model is used to fit 3-site exchange data, the obtained exchange parameters are a function of the B_1 fields used, Fig. 3b. Of interest, for the simulations considered here (see "Materials and methods" for details) we find that as data from larger B_1 fields are included the populations and rates move more closely to those characterizing the $G \underset{k_{E1G}}{\overset{k_{GE1}}{\rightleftharpoons}} E1$ portion of the 3-site exchange reaction. We have fitted our experimental data focusing on all residues with $|\Delta\varpi| > 2$ ppm to a 2-site model and obtained the $\{p_E, k_{ex}\}$ distribution shown in Fig. 3c that is very similar to what is generated with the 'in-silico' 3-site exchange data of Fig. 3b. The extracted exchange parameters for the various combinations of data obtained at different B_o and $^{13}C^{\alpha}$ B_1 fields are summarized in Table 2 showing the same trends as observed in our simulations. This provides further evidence that indeed the exchange process observed in the Im7 protein is more complex than 2-state.

In order to extract accurate exchange parameters, a 3-site exchange model must be used. Indeed, we have tried such an approach. However, the recorded $^{13}C^{\alpha}$ CEST data sets are not of sufficiently high signal-to-noise to extract robust exchange parameters even in fits including data sets

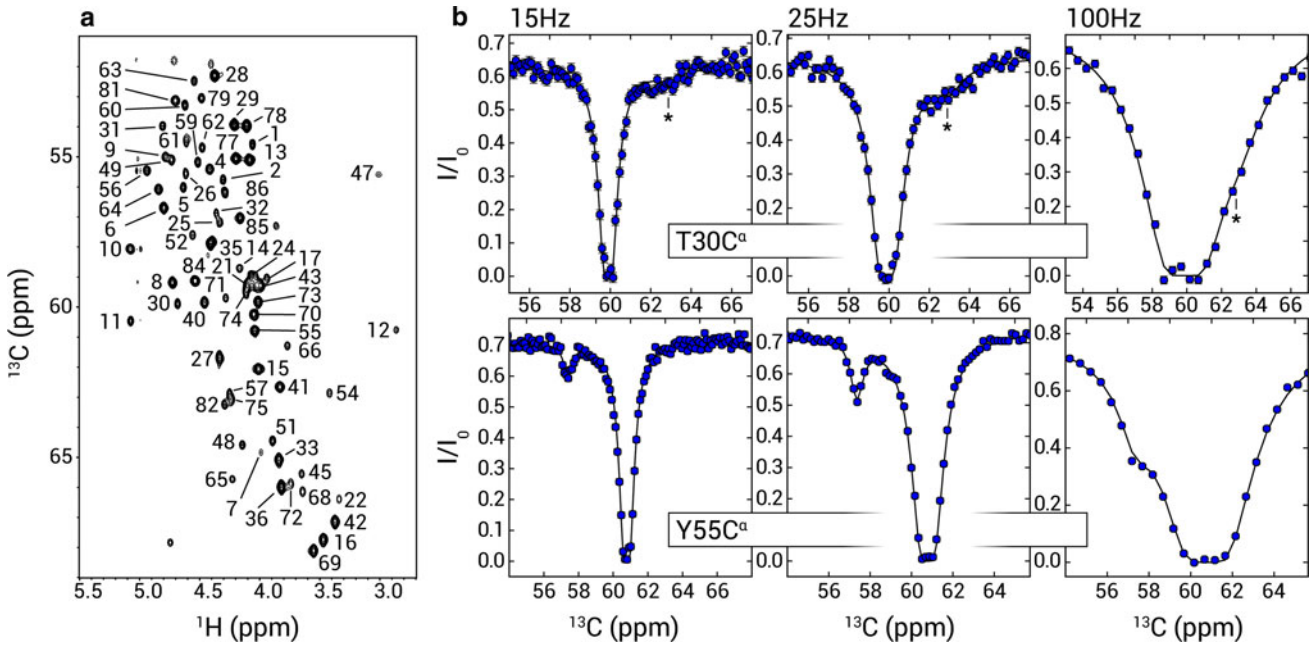

Fig. 2 **a** 2D ^{13}C-^{1}H spectrum of Im7, 18.8 T, 5 °C recorded with the scheme of Fig. 1 and $T_{Ex} = 0$. Peak assignments are indicated. **b** Representative CEST profiles for T30 (*top*) and Y55 (*bottom*). From *left* to *right* are traces recorded with $^{13}C^{\alpha}$ B_1 fields of 15, 25, and 100 Hz, as indicated. Additional experimental details are provided in the text and in Table 1. The *solid line* represents the best-fit solution obtained as described in "Materials and methods". The dip corresponding to the minor state for T30 is indicated by an *asterisk* for clarity

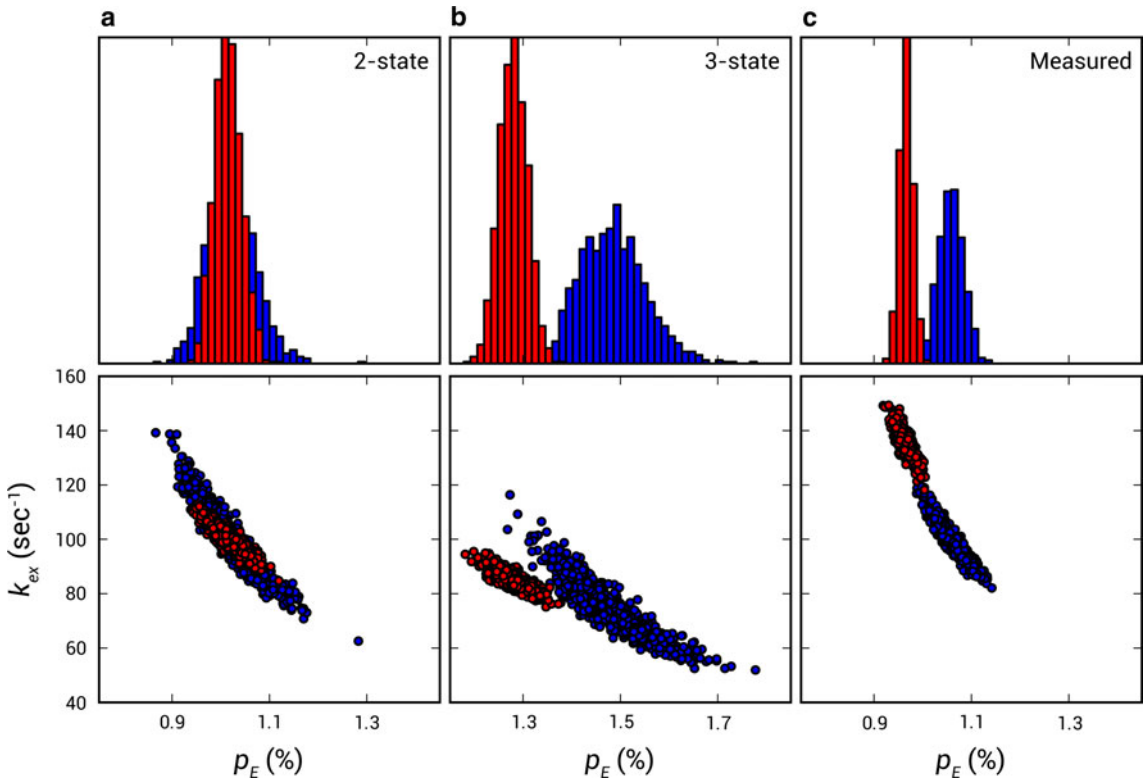

Fig. 3 Monte Carlo simulations (Press et al. 2007) using synthetic 2-state (*left*) and 3-state (center) data sets derived from computations using parameters indicated in "Materials and methods". 1000 data sets are constructed that are subsequently fit to a 2-site exchange model to produce the $\{p_E, k_{ex}\}$ distributions shown. An additional Monte Carlo simulation was also performed using the best-fit solutions to the experimental data (fits of profiles corresponding to the 12 Im7 residues with $|\Delta\varpi| > 2$ ppm) and the experimentally determined intensity errors. The $\{p_E, k_{ex}\}$ distribution so obtained is plotted in the panel on the right. Distributions colored *blue* result from fits of data sets with $^{13}C^{\alpha}$ CEST fields of 15 and 25 Hz; in *red* an additional data set corresponding to a field of 100 Hz is included in the analysis

recorded with different B_1 values. Errors in I/I_o values, quantified as the rmsd of intensities in regions of the CEST profiles for which there are no dips are approximately ± 1.4 % of I_o. That is a factor of 4 larger than errors from ^{15}N-CEST profiles recorded on the A39G FF domain which folds via an on-pathway intermediate (Jemth et al. 2004; Korzhnev et al. 2010) and for which accurate parameters could be extracted from a 3-state fit (unpublished results). As a next best approach we have fitted 7 residues for which $\Delta R_2 \sim 0$ s^{-1} and $|\Delta\varpi| > 2$ ppm to a 2-site exchange model, with the reduced χ^2 surface plotted as a function of k_{ex} (y-axis) and p_E (x-axis) in Fig. 4a. It is clear that k_{ex} and p_E are correlated and that a reasonably broad minimum is obtained. This is made clear by the profiles shown in Fig. 4b, c where values of $\{p_E, k_{ex}\}$ from points *b* and *c* in Fig. 4a have been used in the respective fits. Very similar fits are obtained using both sets of parameters. It is worth noting that despite the large number of offsets measured per CEST profile, the exchange parameters are defined by a small number of points surrounding the excited and ground state correlations so that high signal-to-noise data is required to obtain accurate exchange parameters (errors on the order of ± 0.5 % of I_o).

In our experience, more accurate values of exchange parameters can be extracted from ^{15}N-CEST data and we recommend using this experiment for characterizing the kinetics and thermodynamics of slow exchange processes. Simulations that we have performed, in support of our empirical observations from fits of experimental data described above, indicate that the major limitation with extracting robust exchange parameters (at least for 2-site exchange) is adequate signal-to-noise of the measured data. Unlike the $^{13}C^{\alpha}$ labeling scheme used here, with ^{13}C incorporation at levels ranging between 20–40 % for most residues, ^{15}N-labeled protein samples can be generated with very high levels of enrichment, leading to higher sensitivity spectra. Further increases in sensitivity arise in the ^{15}N-CEST experiment because of narrower ^{15}N linewidths that reflect differences in the relative strengths of $^{13}C^{\alpha}$–$^{1}H^{\alpha}$ and ^{15}N–$^{1}H^{N}$ dipolar interactions ($\sim$2:1).

Because our main interest in the $^{13}C^{\alpha}$-CEST experiment is in obtaining excited state chemical shifts as a first step in structural studies, we were particularly interested in

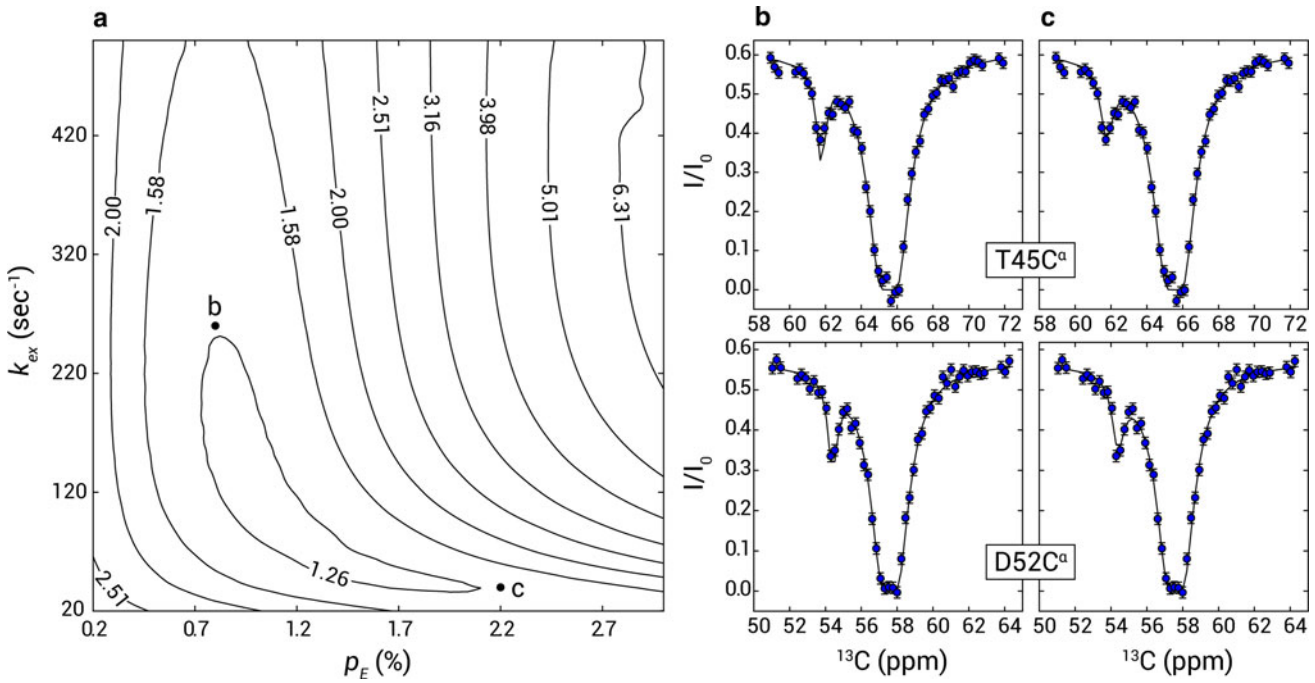

Fig. 4 **a** Reduced χ^2 surface generated from 2-state fits of Im7 $^{13}C^{\alpha}$ CEST profiles of the 7 residues with $|\Delta\varpi| > 2$ ppm and $\Delta R_2 \sim 0$ (*i.e.*, fits did not improve by including ΔR_2). Contours are labeled with their respective reduced χ^2 value. The best reduced χ^2 is found for $p_E = 1.0$ % and $k_{ex} = 120$ s^{-1}. In **b** and **c** are representative fits to CEST data (14.1 T, 25 Hz B_1) from T45 (*top*) and D52 (*bottom*) using the exchange parameters corresponding to points (**b**) and (**c**) indicated on the χ^2 surface in (**a**)

establishing whether uncertainties in $\{p_E, k_{ex}\}$ would degrade the quality of the extracted $\Delta\varpi$ values. Figure 5a presents a linear correlation plot of $\Delta\varpi$ from fits of a pair of $^{13}C^{\alpha}$-CEST data sets recorded with $B_1 = 15, 25$ Hz at 14.1 T (y-axis) versus corresponding values obtained by fitting data sets recorded with $B_1 = 15, 25, 100$ Hz, at 14.1 and 18.8 T. It is clear that an excellent correlation is obtained, with a pair wise rmsd of 0.02 ppm for residues with $|\Delta\varpi| > 0.8$ ppm. For values of $|\Delta\varpi|$ less than $\sim$0.8 ppm there is significant overlap between the major and minor state dips and shift differences are expectedly less well determined, however the correlation is still very high; an rmsd of 0.12 ppm is obtained when all residues are considered. In order to evaluate the accuracy of the extracted shifts we have compared them with those obtained from fits of CPMG dispersion profiles recorded under conditions where the exchange rate lies within the region most sensitive for this technique ($k_{ex} \sim 1{,}000$ s^{-1}, 25 °C). Figure 5b shows that a high correlation is obtained, with small deviations in shifts likely reflecting the different temperatures that were used in recording the two types of data (5 °C, CEST vs 25 °C, CPMG). The rmsd of 0.28 ppm is well under the predictive power for chemical shifts of the $^{13}C^{\alpha}$ carbon using state-of-the-art programs such as SPARTA+ ($\sim$0.9 ppm). Note that an rmsd of 0.28 ppm reflects errors in both CPMG and CEST data, and hence is an upper bound to the uncertainty of CEST excited state chemical shifts.

Concluding remarks

We have presented a new CEST-based experiment for studying slowly exchanging protein systems with rates on the order of 100 s^{-1}. The method makes use of $^{13}C^{\alpha}$ probes, introduced using [2-^{13}C]-glucose as the sole carbon source in protein expression systems to minimize $^{13}C^{\alpha}$–^{13}C couplings. As expected, the sensitivity of the $^{13}C^{\alpha}$-CEST experiment is reduced relative to the ^{15}N-scheme (errors in data approximately 4 fold larger) that influences the quality of the extracted exchange parameters. Nevertheless, accurate $^{13}C^{\alpha}$ chemical shift values of the excited state are readily obtained from data recorded at only a single static magnetic field strength. Given the sensitivity of this class of chemical shift to protein secondary structure and, therefore, the value of $^{13}C^{\alpha}$ restraints for the structure determination of excited protein conformers, it is expected that the presented $^{13}C^{\alpha}$-CEST experiment will assume an important role in studies of rare, but biologically significant, protein conformations.

Supporting information available

One figure showing a linear correlation of $^{13}C^{\alpha}$ ΔR_2 values measured for Im7 (5 °C) from fits of CEST data recorded at 14.1 and 18.8 T, one table of $^{13}C^{\alpha}$ $|\Delta\varpi|$ values for the Im7 protein, along with pulse sequence code for the scheme of Fig. 1.

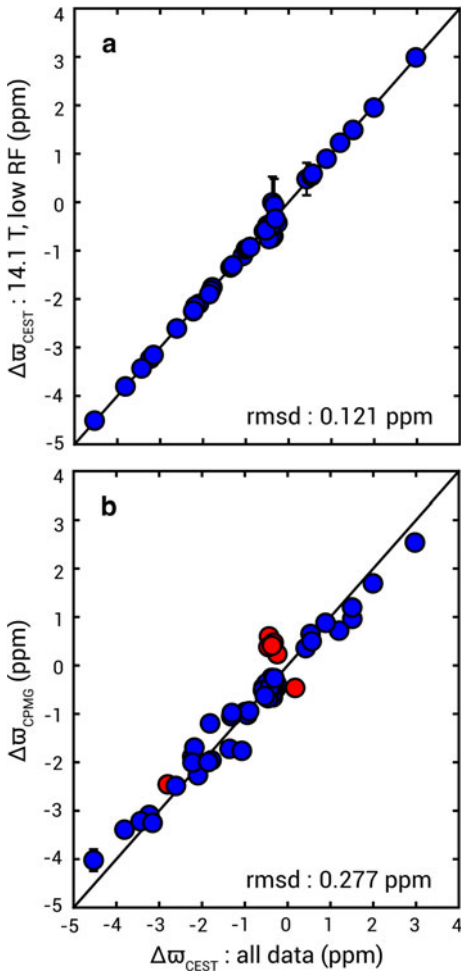

Fig. 5 Linear correlation plots of $\Delta\varpi$ values obtained from analysis of all profiles from 6 CEST datasets (x-axis; see Table 1) vs **a** shift differences based on fits of only two CEST datasets ($^{13}C^{\alpha}$ B_1 fields of 15 and 25 Hz, 14.1 T; y-axis) or **b** $\Delta\varpi$ obtained from fitting CPMG dispersion profiles recorded at 25 °C (y-axis). Points in *red* in (**b**) correspond to cases for which the sign of $\Delta\varpi$ values could not be determined by a comparison of (1) peak positions in HSQC/HMQC spectra (Skrynnikov et al. 2002) or of (2) the offset dependence of $R_{1\rho}$ relaxation rates (Auer et al. 2010) that are the approaches of choice to obtain the sign of shift differences obtained from fits of CPMG data. Root-mean-square-deviations (rmsd) shown in the *bottom right* of the plots are calculated for all signed data

Acknowledgments The authors thank Dr. Sara Whittaker and Professors Geoff Moore and Sheena Radford for the gift of Im7 plasmids. A.L.H. acknowledges the National Science Foundation (OISE-0852964) and the Canadian Institutes of Health Research (CIHR) training grant in protein folding and disease for post-doctoral support. This work was supported by grants from the CIHR and the Natural Sciences and Engineering Research Council of Canada (LEK). L.E.K. holds a Canada Research Chair in Biochemistry.

References

Allerhand A, Gutowsky HS (1964) Spin—Echo NMR studies of chemical exchange. I. Some general aspects. J Chem Phys 41:2115. doi:10.1063/1.1726215

Auer R, Hansen DF, Neudecker P, Korzhnev DM, Muhandiram DR, Konrat R, Kay LE (2010) Measurement of signs of chemical shift differences between ground and excited protein states: a comparison between H(S/M)QC and R1rho methods. J Biomol NMR 46:205–216. doi:10.1007/s10858-009-9394-z

Bai Y, Sosnick TR, Mayne L, Englander SW (1995) Protein folding intermediates: native-state hydrogen exchange. Science 269:192–197. doi:10.1126/science.7618079

Boehr DD, Wright PE (2008) Biochemistry. How do proteins interact? Science 320:1429–1430. doi:10.1126/science.1158818

Bouvignies G, Kay LE (2012a) A 2D ^{13}C-CEST experiment for studying slowly exchanging protein systems using methyl probes: an application to protein folding. J Biomol NMR 53:303–310. doi:10.1007/s10858-012-9640-7

Bouvignies G, Kay LE (2012b) Measurement of proton chemical shifts in invisible states of slowly exchanging protein systems by chemical exchange saturation transfer. J Phys Chem B 116: 14311–14317. doi:10.1021/jp311109u

Bouvignies G, Vallurupalli P, Hansen DF, Correia BE et al (2011) Solution structure of a minor and transiently formed state of a T4 lysozyme mutant. Nature 477:111. doi:10.1038/nature10349

Brockwell DJ, Radford SE (2007) Intermediates: ubiquitous species on folding energy landscapes? Curr Opin Struct Biol 17:30–37. doi:10.1016/j.sbi.2007.01.003

Camilloni C, Robustelli P, De Simone A, Cavalli A, Vendruscolo M (2012) Characterization of the conformational equilibrium between the two major substates of RNase a using NMR chemical shifts. J Am Chem Soc 134:3968–3971. doi:10.1021/ja210951z

Capaldi AP, Shastry MC, Kleanthous C, Roder H, Radford SE (2001) Ultrarapid mixing experiments reveal that Im7 folds via an on-pathway intermediate. Nat Struct Biol 8:68–72. doi:10.1038/83074

Capaldi AP, Kleanthous C, Radford SE (2002) Im7 folding mechanism: misfolding on a path to the native state. Nat Struct Biol 9:209–216. doi:10.1038/nsb757

Carr HY, Purcell EM (1954) Effects of diffusion on free precession in nuclear magnetic resonance experiments. Phys Rev 94:630–638. doi:10.1103/PhysRev.94.630

Cavalli A, Salvatella X, Dobson CM, Vendruscolo M (2007) Protein structure determination from NMR chemical shifts. Proc Natl Acad Sci USA 104:9615–9620. doi:10.1073/pnas.0610313104

Chiti F, Dobson CM (2006) Protein misfolding, functional amyloid, and human disease. Annu Rev Biochem 75:333–366. doi:10.1146/annurev.biochem.75.101304.123901

Daggett V, Fersht A (2003) The present view of the mechanism of protein folding. Nat Rev Mol Cell Biol 4:497–502. doi:10.1038/nrm1126

Delaglio F, Grzesiek S, Vuister GW, Zhu G, Pfeifer J, Bax A (1995) NMRPipe: a multidimensional spectral processing system based on UNIX pipes. J Biomol NMR 6:277–293. doi:10.1007/BF00197809

Dethoff EA, Petzold K, Chugh J, Casiano-Negroni A, Al-Hashimi HM (2012) Visualizing transient low-populated structures of RNA. Nature 491:724–728. doi:10.1038/nature11498

Deverell C, Morgan RE, Strange JH (1970) Studies of chemical exchange by nuclear magnetic relaxation in the rotating frame. Mol Phys 18:553–559. doi:10.1080/00268977000100611

Fawzi NL, Ying J, Ghirlando R, Torchia DA, Clore GM (2011) Atomic-resolution dynamics on the surface of amyloid-β protofibrils probed by solution NMR. Nature 480:268–272. doi:10.1038/nature10577

Forsén S, Hoffman RA (1963) Study of moderately rapid chemical exchange reactions by means of nuclear magnetic double resonance. J Chem Phys 39:2892. doi:10.1063/1.1734121

Fraser JS, Clarkson MW, Degnan SC, Erion R, Kern D, Alber T (2009) Hidden alternative structures of proline isomerase

essential for catalysis. Nature 462:669–673. doi:10.1038/nature08615

Freeman R, Kempsell SP, Levitt MH (1980) Radiofrequency pulse sequences which compensate their own imperfections. J Magn Reson 38:453–479. doi:10.1016/0022-2364(80)90327-3

Guenneugues M, Berthault P, Desvaux H (1999) A method for determining B1 field inhomogeneity. Are the biases assumed in heteronuclear relaxation experiments usually underestimated? J Magn Reson 136:118–126. doi:10.1006/jmre.1998.1590

Han B, Liu Y, Ginzinger SW, Wishart DS (2011) SHIFTX2: significantly improved protein chemical shift prediction. J Biomol NMR. doi:10.1007/s10858-011-9478-4

Hansen AL, Kay LE (2011) Quantifying millisecond time-scale exchange in proteins by CPMG relaxation dispersion NMR spectroscopy of side-chain carbonyl groups. J Biomol NMR 50:347–355. doi:10.1007/s10858-011-9520-6

Hansen DF, Vallurupalli P, Kay LE (2008a) Using relaxation dispersion NMR spectroscopy to determine structures of excited, invisible protein states. J Biomol NMR 41:113–120. doi:10.1007/s10858-008-9251-5

Hansen DF, Vallurupalli P, Kay LE (2008b) An improved 15 N relaxation dispersion experiment for the measurement of millisecond time-scale dynamics in proteins. J Phys Chem B 112:5898–5904. doi:10.1021/jp074793o

Hansen DF, Vallurupalli P, Lundström P, Neudecker P, Kay LE (2008c) Probing chemical shifts of invisible states of proteins with relaxation dispersion NMR spectroscopy: how well can we do? J Am Chem Soc 130:2667–2675. doi:10.1021/ja078337p

Hansen AL, Nikolova EN, Casiano-Negroni A, Al-Hashimi HM (2009) Extending the range of microsecond-to-millisecond chemical exchange detected in labeled and unlabeled nucleic acids by selective carbon R1(rho) NMR spectroscopy. J Am Chem Soc 131:3818–3819. doi:10.1021/ja8091399

Hansen AL, Lundström P, Velyvis A, Kay LE (2012) Quantifying millisecond exchange dynamics in proteins by CPMG relaxation dispersion NMR using side-chain (1)H Probes. J Am Chem Soc 134:3178–3189. doi:10.1021/ja210711v

Ishima R, Freedberg DI, Wang Y-X, Louis JM, Torchia DA (1999) Flap opening and dimer-interface flexibility in the free and inhibitor-bound HIV protease, and their implications for function. Structure 7:1047–1055. doi:10.1016/S0969-2126(99)80172-5

Ishima R, Baber JL, Louis JM, Torchia DA (2004) Carbonyl carbon transverse relaxation dispersion measurements and ms-micros timescale motion in a protein hydrogen bond network. J Biomol NMR 29:187–198. doi:10.1023/B:JNMR.0000019249.50306.5d

Iwadate M, Asakura T, Williamson MP (1999) C alpha and C beta carbon-13 chemical shifts in proteins from an empirical database. J Biomol NMR 13:199–211. doi:10.1023/A:1008376710086

Jemth P, Gianni S, Day R, Li B, Johnson CM, Daggett V, Fersht AR (2004) Demonstration of a low-energy on-pathway intermediate in a fast-folding protein by kinetics, protein engineering, and simulation. Proc Natl Acad Sci USA 101:6450–6455. doi:10.1073/pnas.0401732101

Karplus M, Kuriyan J (2005) Molecular dynamics and protein function. Proc Natl Acad Sci USA 102:6679–6685. doi:10.1073/pnas.0408930102

Kay LE, Keifer P, Saarinen T (1992) Pure absorption gradient enhanced heteronuclear single quantum correlation spectroscopy with improved sensitivity. J Am Chem Soc 114:10663–10665. doi:10.1021/ja00052a088

Kneller DG, Kuntz ID (1993) UCSF Sparky: an NMR display, annotation and assignment tool. J Cell Biochem 53(S17C):254. doi:10.1002/jcb.240530709

Kohlhoff KJ, Robustelli P, Cavalli A, Salvatella X, Vendruscolo M (2009) Fast and accurate predictions of protein NMR chemical shifts from interatomic distances. J Am Chem Soc 131:13894–13895. doi:10.1021/ja903772t

Korzhnev DM, Salvatella X, Vendruscolo M, Di Nardo AA, Davidson AR, Dobson CM, Kay LE (2004) Low-populated folding intermediates of Fyn SH3 characterized by relaxation dispersion NMR. Nature 430:586–590. doi:10.1038/nature02655

Korzhnev DM, Mittermaier AK, Kay LE (2005) Cross-correlated spin relaxation effects in methyl 1H CPMG-based relaxation dispersion experiments: complications and a simple solution. J Biomol NMR 31:337–342. doi:10.1007/s10858-005-2468-7

Korzhnev DM, Religa TL, Banachewicz W, Fersht AR, Kay LE (2010) A transient and low-populated protein-folding intermediate at atomic resolution. Science 329:1312–1316. doi:10.1126/science.1191723

Lange OF, Rossi P, Sgourakis NG, Song Y et al (2012) Determination of solution structures of proteins up to 40 kDa using CS-Rosetta with sparse NMR data from deuterated samples. Proc Natl Acad Sci USA 109:10873–10878. doi:10.1073/pnas.1203013109

Levitt MH (1982) Symmetrical composite pulse sequences for NMR population inversion. II. Compensation of resonance offset. J Magn Reson 50:95–110. doi:10.1016/0022-2364(82)90035-X

Lundström P, Teilum K, Carstensen T, Bezsonova I, Wiesner S, Hansen DF, Religa TL, Akke M, Kay LE (2007a) Fractional 13C enrichment of isolated carbons using [1-13C]- or [2- 13C]-glucose facilitates the accurate measurement of dynamics at backbone Calpha and side-chain methyl positions in proteins. J Biomol NMR 38:199–212. doi:10.1007/s10858-007-9158-6

Lundström P, Vallurupalli P, Religa TL, Dahlquist FW, Kay LE (2007b) A single-quantum methyl 13C-relaxation dispersion experiment with improved sensitivity. J Biomol NMR 38:79–88. doi:10.1007/s10858-007-9149-7

Lundström P, Hansen DF, Kay LE (2008) Measurement of carbonyl chemical shifts of excited protein states by relaxation dispersion NMR spectroscopy: comparison between uniformly and selectively (13)C labeled samples. J Biomol NMR 42:35–47. doi:10.1007/s10858-008-9260-4

Lundström P, Hansen DF, Vallurupalli P, Kay LE (2009) Accurate measurement of alpha proton chemical shifts of excited protein states by relaxation dispersion NMR spectroscopy. J Am Chem Soc 131:1915–1926. doi:10.1021/ja807796a

Marion D, Ikura M, Bax A (1989) Improved solvent suppression in one- and two-dimensional NMR spectra by convolution of time-domain data. J Magn Reson 84:425–430. doi:10.1016/0022-2364(89)90391-0

McConnell HM (1958) Reaction rates by nuclear magnetic resonance. J Chem Phys 28:430. doi:10.1063/1.1744152

Meiboom S, Gill D (1958) Modified spin-echo method for measuring nuclear relaxation times. Rev Sci Instrum 29:688. doi:10.1063/1.1716296

Neudecker P, Robustelli P, Cavalli A, Walsh P, Lundström P, Zarrine-Afsar A, Sharpe S, Vendruscolo M, Kay LE (2012) Structure of an intermediate state in protein folding and aggregation. Science 336:362–366. doi:10.1126/science.1214203

Nikolova EN, Kim E, Wise AA, O'Brien PJ, Andricioaei I, Al-Hashimi HM (2011) Transient Hoogsteen base pairs in canonical duplex DNA. Nature. doi:10.1038/nature09775

Orekhov VY, Korzhnev DM, Kay LE (2004) Double- and zero-quantum NMR relaxation dispersion experiments sampling millisecond time scale dynamics in proteins. J Am Chem Soc 126:1886–1891. doi:10.1021/ja038620y

Palmer AG, Massi F (2006) Characterization of the dynamics of biomacromolecules using rotating-frame spin relaxation NMR spectroscopy. Chem Rev 106:1700–1719. doi:10.1021/cr0404287

Palmer AG, Grey MJ, Wang C (2005) Solution NMR spin relaxation methods for characterizing chemical exchange in high-

molecular-weight systems. Methods Enzymol 394:430–465. doi:10.1016/S0076-6879(05)94018-4

Papadakos G, Wojdyla JA, Kleanthous C (2012) Nuclease colicins and their immunity proteins. Q Rev Biophys 45:57–103. doi:10.1017/S0033583511000114

Parisien M, Major F (2008) The MC-Fold and MC-Sym pipeline infers RNA structure from sequence data. Nature 452:51–55. doi:10.1038/nature06684

Press WH, Teukolsky SA, Vetterling WT, Flannery BP (2007) Numerical recipes : the art of scientific computing, 3rd edn. Cambridge University Press, Cambridge

Robustelli P, Kohlhoff KJ, Cavalli A, Vendruscolo M (2010) Using NMR chemical shifts as structural restraints in molecular dynamics simulations of proteins. Structure 18:923–933. doi:10.1016/j.str.2010.04.016

Santoro J, King GC (1992) A constant-time 2D overbodenhausen experiment for inverse correlation of isotopically enriched species. J Magn Reson 97:202–207. doi:10.1016/0022-2364(92)90250-B

Sattler M, Schleucher J, Griesinger C (1999) Heteronuclear multidimensional NMR experiments for the structure determination of proteins in solution employing pulsed field gradients. Prog Nucl Magn Reson Spectrosc 34:93–158. doi:10.1016/S0079-6565(98)00025-9

Schleucher J, Sattler M, Griesinger C (1993) Coherence selection by gradients without signal attenuation: application to the three-dimensional HNCO experiment. Angew Chem Int Ed Engl 32:1489–1491. doi:10.1002/anie.199314891

Shaka AJ, Keeler J, Frenkiel T, Freeman R (1983) An improved sequence for broadband decoupling: WALTZ-16. J Magn Reson 52:335–338. doi:10.1016/0022-2364(83)90207-X

Shaka AJ, Barker PB, Freeman R (1985) Computer-optimized decoupling scheme for wideband applications and low-level operation. J Magn Reson 64:547–552. doi:10.1016/0022-2364(85)90122-2

Shaka AJ, Lee CJ, Pines A (1988) Iterative schemes for bilinear operators; application to spin decoupling. J Magn Reson 77:274–293. doi:10.1016/0022-2364(88)90178-3

Shen Y, Bax A (2010) SPARTA + : a modest improvement in empirical NMR chemical shift prediction by means of an artificial neural network. J Biomol NMR 48:13–22. doi:10.1007/s10858-010-9433-9

Skrynnikov NR, Dahlquist FW, Kay LE (2002) Reconstructing NMR spectra of "invisible" excited protein states using HSQC and HMQC experiments. J Am Chem Soc 124:12352–12360. doi:10.1021/ja0207089

Spera S, Bax A (1991) Empirical correlation between protein backbone conformation and C.alpha. and C.beta. 13C nuclear magnetic resonance chemical shifts. J Am Chem Soc 113:5490–5492. doi:10.1021/ja00014a071

Vallurupalli P, Hansen DF, Kay LE (2008) Structures of invisible, excited protein states by relaxation dispersion NMR spectroscopy. Proc Natl Acad Sci USA 105:11766–11771. doi:10.1073/pnas.0804221105

Vallurupalli P, Bouvignies G, Kay LE (2011) Increasing the exchange time-scale that can be probed by cpmg relaxation dispersion NMR. J Phys Chem B. doi:10.1021/jp209610v

Vallurupalli P, Bouvignies G, Kay LE (2012) Studying "invisible" excited protein states in slow exchange with a major state conformation. J Am Chem Soc 134:8148–8161. doi:10.1021/ja3001419

Vila JA, Scheraga HA (2009) Assessing the accuracy of protein structures by quantum mechanical computations of 13C(alpha) chemical shifts. Acc Chem Res 42:1545–1553. doi:10.1021/ar900068s

Vila JA, Villegas ME, Baldoni HA, Scheraga HA (2007) Predicting 13Calpha chemical shifts for validation of protein structures. J Biomol NMR 38:221–235. doi:10.1007/s10858-007-9162-x

Vuister GW, Bax A (1992) Resolution enhancement and spectral editing of uniformly 13C-enriched proteins by homonuclear broadband 13C decoupling. J Magn Reson 98:428–435. doi:10.1016/0022-2364(92)90144-V

Wishart DS, Sykes BD (1994) The 13C chemical-shift index: a simple method for the identification of protein secondary structure using 13C chemical-shift data. J Biomol NMR 4:171–180. doi:10.1007/BF00175245

Wishart DS, Arndt D, Berjanskii M, Tang P, Zhou J, Lin G (2008) CS23D: a web server for rapid protein structure generation using NMR chemical shifts and sequence data. Nucleic Acids Res 36:W496–W502. doi:10.1093/nar/gkn305